Seasonality of the Migrating Semidiurnal Tide in the Tropical Upper Mesosphere and Lower Thermosphere and its Thermodynamic and Momentum Budget

Cornelius Csar Jude H. Salinas[1,2], Dong L. Wu[3], Jae N. Lee[4], Loren C. Chang[1,2], Liying Qian[5] and Hanli Liu[5]

[1]*Department of Space Science and Engineering, National Central University, Zhongli, Taiwan*

[2]*Center for Astronautical Physics and Engineering, National Central University, Zhongli, Taiwan*

[3]*NASA Goddard Space Flight Center, Greenbelt, Maryland, USA*

[4]*Joint Center for Earth Systems Technology, University of Maryland, Baltimore County, Baltimore, Maryland, USA*

[5] *National Center for Atmospheric Research High Altitude Observatory, Boulder, Colorado, USA*

Corresponding author: Loren C. Chang, Department of Space Science and Engineering, National Central University, Zhongli District, Taoyuan City, Taiwan (loren@g.ncu.edu.tw)

Abstract

This work uses the Specified Dynamics – Whole Atmosphere Community Climate Model with Ionosphere/Thermosphere eXtension (SD-WACCM-X) to determine and explain the seasonality of the migrating semidiurnal tide (SW2) components of tropical upper mesosphere and lower thermosphere (UMLT) temperature, zonal-wind and meridional-wind. This work also quantifies aliasing due to SW2 in satellite-based tidal estimates. Results show that during equinox seasons, the vertical profile of tropical UMLT temperature SW2 and zonal wind SW2's

amplitudes have a double peak structure while they, along with meridional wind SW2, have a single peak structure in their amplitudes in June solstice. Hough mode reconstruction reveals that a linear combination of 5 SW2 Hough modes cannot fully reproduced these features. Tendency analysis reveals that for temperature, the adiabatic term, non-linear advection term and linear advection term are important. For the winds, the classical terms, non-linear advection term, linear advection term and gravity wave drag are important. Results of our alias analysis then indicate that SW2 can induce an ~60% alias in zonal-mean and DW1 components calculated from sampling like that of the Thermosphere Ionosphere Mesosphere Energetics and Dynamics satellite and the Aura satellite. This work concludes that in-situ generation by wave-wave interaction and/or by gravity waves play significant roles in the seasonality of tropical UMLT temperature SW2, zonal wind SW2 and meridional wind SW2. The alias analysis further adds that one cannot simply assume SW2 in the tropical UMLT is negligible.

Index Terms/ Keywords: Tides, Mesosphere, Lower Thermosphere

Key Points:

- Thermodynamic and momentum budget of tropical migrating semidiurnal tide in the upper mesosphere and lower thermosphere calculated.
- Hough modes cannot fully reconstruct tropical migrating semidiurnal tide component of temperature and winds.
- Wave-wave interaction and gravity waves significantly affect tropical migrating semidiurnal tide component of temperature and winds.

1. Introduction

The solar migrating semidiurnal tide (SW2) is a westward propagating wavenumber-2 planetary-scale wave with a period of 12 hours. Studies have shown that the solar absorption of stratospheric ozone primarily generates SW2 (Chapman and Lindzen, 1970; Forbes and Garret, 1979). Its long wavelength allows it to vertically propagate up to the ionosphere/thermosphere (I/T) region (Chapman and Lindzen, 1970). While it propagates, it has been shown to interact with the background atmosphere and/or atmospheric waves such as planetary-scale waves and gravity waves (Lindzen and Hong, 1974; Walterscheid and Venkateswaran, 1979a, b; Forbes, 1982; Teitelbaum et al, 1989; Teitelbaum and Vial, 1991; Forbes et al, 1995; Palo et al, 1999; Angelats I Coll and Forbes, 2002; Yamashita et al, 2002; Forbes and Wu, 2006; Forbes et al, 2008; Pedatella and Forbes, 2010; Zhang et al, 2021; van Caspel et al, 2021).

SW2 in the tropical upper mesosphere and lower thermosphere (UMLT) region is largely ignored because most studies focus on SW2's variability in the middle to high latitude UMLT where its amplitudes are known to be the largest (Manson et al, 2002; Wu et al, 2011). These studies often analyze the interactions of SW2 with winter-prominent phenomena like sudden stratospheric warmings and stationary planetary-scale waves (Teitelbaum et al, 1989; Teitelbaum and Vial, 1991; Palo et al, 1999; Angelats I Coll and Forbes, 2002; Yamashita et al, 2002; Forbes and Wu, 2006; Forbes et al, 2008; Pedatella and Forbes, 2010; Limpasuvan et al, 2016; Zhang et al, 2021; van Caspel et al, 2021).

The motivation of this work are studies showing that the 12-hour component of horizontal winds in the tropics observed by ground-based instruments exhibit noteworthy amplitudes and variabilities that three-dimensional models cannot reproduce. Numerous ground-based instruments have observed that the 12-hour oscillation component of tropical UMLT

horizontal winds (between 85 and 100 km) exhibit significant altitudinal variations. Observations also show that localized peak amplitudes of these 12-hour oscillation are comparable to the amplitudes of the often more dominant 24-hour oscillations (Reddi and Ramkumar, 1997; Vincent et al, 1998; Manson et al, 1999; Deepa et al, 2006). Reddi and Ramkumar (1997) and Deepa et al (2006) reported that meteor wind radar (MWR) observations of 12-hour oscillations in zonal and meridional winds at Trivandrum (latitude 8N) from 1984 to 1988 had, for all seasons, significant altitudinal variations present in the 12-hour oscillation amplitude vertical profiles. They then compared them with 24-hour oscillation amplitudes and found that the 12-hour amplitudes exhibited local peaks with magnitudes comparable to the 24-hour oscillations. Vincent et al (1998) and Manson et al (1999) reported medium frequency radar (MFR) observations of 12-hour oscillations in horizontal winds at Christmas Island (latitude 2N) and Hawaii (latitude 22N) and found something like the observations at Trivandrum. These studies also presented the phases of these 12-hour oscillations. These phases indicated that wavelengths were consistently greater than 100 km (Reddi and Ramkumar, 1997; Vincent et al, 1998; Manson et al, 1999; Deepa et al, 2006).

Studies that compared these ground-based observations with linear models showed that the linear models such as the Forbes and Vial (1989) tidal model and the Global Scale Wave Model (GSWM) could not reproduce the significant altitudinal variation in 12-hour oscillation amplitudes. These models consistently simulated 12-hour oscillation amplitude profiles exhibiting only an exponential increase with height (Reddi and Ramkumar, 1997; Vincent et al, 1998; Manson et al, 1999; Deepa et al, 2006). Local maximum peaks weren't found between 80 and 100 km. Their simulated phases also differed from observations. Their simulated phases indicated shorter vertical wavelengths. On the other hand, three-dimensional (3D) first principles

atmospheric general circulation models simulated 12-hour oscillations whose amplitudes exhibited local-peaks between 85 and 100 km (Du et al, 2007; Ravis et al, 2013). Ravis et al (2013) compared horizontal wind observations in Ascension Island (latitude 8S) from 2002 to 2011 with simulations from three-dimensional whole atmosphere models called the Canadian Middle Atmosphere Model (CMAM) and the Specified Dynamics – Whole Atmosphere Community Climate Model (SD-WACCM). Their results show the simulations exhibiting significantly more altitudinal variation in the 12-hour oscillations amplitude although the variation isn't the same as observed. Their results also showed that WACCM 12-hour oscillation phases were indicative of the (2,2) mode. However, their work doesn't determine the contributions of SW2 in these 12-hour oscillations. On the other hand, Du et al (2007) analyzed 12-hour oscillations from meteor radar observations in Jakarta (latitude 6S) and Kotobabang (latitude 0) and compared them with CMAM simulations. They found that the SW2 component does contribute the most to the 12-hour oscillations in these regions. The ability of three-dimensional models to, at the very least, capture the significant altitude variation of SW2's amplitude over the tropics indicates that non-classical and non-linear processes may primarily drive SW2 in the tropics. No study has analyzed this in-depth.

Space-based instruments that can resolve the SW2 component of horizontal winds in the tropical UMLT include the High Resolution Doppler Imager (HRDI) onboard the Upper Atmosphere Research Satellite (UARS) as well as the Thermosphere-Ionosphere-Mesosphere Energetics and Dynamics (TIMED) Doppler Interferometer (TIDI) instrument onboard the TIMED satellite (Burrage et al., 1995a; Burrage et al., 1995b; McLandress et al., 1994, 1996; Wu et al., 2003; Forbes and Wu, 2006; Zhang et al, 2006; Wu et al., 2006; Oberheide et al., 2007; Forbes et al, 2008; Yuan et al., 2008; Pancheva et al, 2009). Unfortunately, nobody has

done any in-depth analysis of the SW2 component of horizontal winds solely in the tropical UMLT region with these instruments because, as mentioned earlier, focus has always been on the regions where amplitudes are the highest which are over the middle to high latitudes.

Doing an in-depth analysis of SW2 in the tropical UMLT region is important in fully understanding the dynamics in the region. This is crucial to accurate space weather forecasting. Wave-wave interaction in the region continues to be difficult to understand and to forecast. Numerous studies have already shown that traveling planetary waves from other latitudes interact with the most dominant migrating tide in the UMLT region, the migrating diurnal tide (Chang et al, 2011; Forbes and Zhang, 2017). On the other hand, minimal work presents an understanding on how these waves interact with SW2 because its amplitude is weak in this region. However, based on the aforementioned studies using ground-based instruments, linear models and three-dimensional models, there are altitudes in the tropical UMLT where SW2's amplitudes may be significant enough that it could be involved in wave-wave interactions with other planetary waves. In the middle to high latitudes, SW2 has been shown to interact with these planetary scale waves and form non-migrating tides (Teitelbaum et al, 1989; Teitelbaum and Vial, 1991; Palo et al, 1999; Angelats I Coll and Forbes, 2002; Yamashita et al, 2002; Forbes and Wu, 2006; Forbes et al, 2008; Pedatella and Forbes, 2010; Limpasuvan et al, 2016; Zhang et al, 2021; van Caspel et al, 2021). Thus, understanding this complexity in SW2's amplitudes over the tropical MLT is important in knowing more of these other wave-wave interactions.

Doing an in-depth analysis of SW2 in the tropical UMLT region is also important in analyzing satellite measurements with limited local-time coverages. Two-dimensional least-squares fit is one of the more reliable ways to estimate both the daily-mean zonal-mean component and atmospheric wave components of a given atmospheric parameter if the data

achieves full local-time coverage (Wu et al, 1995). This method mitigates aliasing. However, for the analysis of short-term variabilities, other methods are currently being utilized that tend to make assumptions on the presence of particular atmospheric waves (Oberheide et al, 2003). One well-known approach is applied on observations from sun-synchronous satellites. These sun-synchronous satellites typically only provide global observations at two local-times. Over the equator, these local times are around 12 hours apart. To get the daily-mean zonal-mean profile for a day, studies commonly just average these values with the assumption that SW2 is negligible. This is done with the assumption that SW2 amplitudes are negligible, and this assumption is believed to always be true over the equator even though minimal work has been done to investigate SW2 in the region.

This work aims to further our understanding of SW2 by investigating the seasonality of SW2 in the tropical UMLT using the Specified Dynamics – Whole Atmosphere Community Climate Model with Ionosphere/Thermosphere eXtension (SD-WACCM-X). Using a multi-year run of SD-WACCM-X that spans from 2000 to 2019, this work determines the seasonal climatology of the SW2 component of UMLT temperature and horizontal winds averaged over the tropics. Then, this work determines its physical mechanisms by quantifying the contributions of Hough modes to these features as well as determining the thermodynamic and momentum budget behind these features. Finally, we quantify the tidal aliases involving SW2 when one uses satellite-based instruments. Since observational studies have ignored SW2 over the tropics, nobody has done any thorough analysis of tidal aliases involving SW2. We are specifically going to determine the alias due to the most dominant tide in this region, the migrating diurnal tide (DW1). By doing all these analyses, this work not only aims to further our understanding of SW2

in the tropical UMLT region, but this work also aims to be a springboard for in-depth analysis of SW2 in this region using satellite-based observations.

2. Methodology

There are two parts in our analysis. The first part presents and explains the seasonality of SD-WACCM-X SW2 in tropical UMLT temperature, zonal wind and meridional wind. The second part is an alias test to quantify the aliasing involving SW2. In this section, we first present the model and the diagnostics involved in presenting explaining the seasonality of SD-WACCM-X SW2. The second part presents the observations used for the alias analysis as well as the alias test.

2.1 SD-WACCM-X Simulations and Diagnostics

2.1.1 SD-WACCM-X Model

WACCM-X is a first-principles Physics-based model that simulates the whole atmosphere from the surface to the Ionosphere/Thermosphere while accounting for the coupling of the atmosphere with the ocean, sea ice and land. Ravis et al (2007) showed that the WACCM can simulate SW2 amplitudes in the tropical E-region that exhibited local maxima. WACCM simulates the atmosphere from the surface to around 140 km. WACCM's tropical E-region, which is between 90 km and 110 km, contains minimal ionosphere electrodynamics. On the other hand, WACCM-X simulates the atmosphere from the surface to around 700 km and it incorporates a more accurate ionosphere. For more descriptions on the model, see Liu et al (2018a; 2018b). WACCM-X is a model that combines WACCM with elements of the thermosphere ionosphere general circulation models. SD-WACCM-X is a version of the WACCM-X that is nudged by the Modern-Era Retrospective Analysis for Research and Applications (MERRA) Reanalysis dataset from the

surface to around 50 km (*Rienecker et al*, 2011; *Marsh et al*, 2013). This ensures that the atmosphere from the surface to the stratosphere is realistic in all simulations. We build off Ravis et al (2007) by utilizing a model with more accurate ionosphere as well as by doing a more in-depth analysis of SW2's seasonality in the tropical E-region.

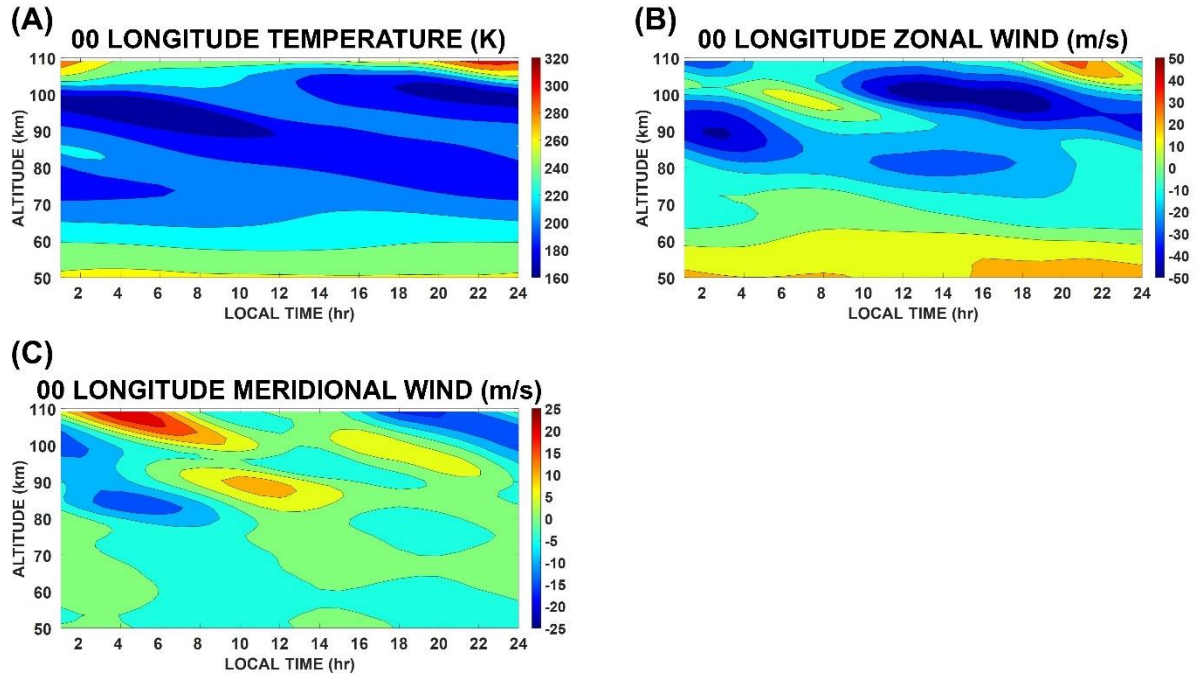

Figure 1: March Equinox SD-WACCM-X temperature (A), zonal wind (B) and meridional wind (C) averaged between latitudes 10S and 10N and at longitude 0 as a function of altitude and local-time.

We ran the model from 2000 to 2019 with a horizontal resolution of 1.9° in latitude and 2.5° in longitude and a vertical resolution of 2 points per scale height below ~50 km and 4 points per scale height above ~50 km. We then calculated the monthly means of all the output variables from these simulations. From these monthly means, we calculated the seasonal climatology of each parameter. For example, when this paper mentions temperature in March, this refers to

averages of temperature for all March months between 2002 and 2019. We then performed our analysis and model diagnostics on these monthly-mean parameters.

Atmospheric tides are global phenomena. Hence, to fully resolve them, one needs a dataset that attains global and full local-time coverage in a day (Oberheide et al, 2003). Unfortunately, no such observational dataset exists. Ground-based instruments can give you full local-time coverage in a day but not global coverage. Figure 1 shows the altitude-local time profiles of March temperature, zonal wind and meridional wind averaged between latitudes 10S and 10N over 0-degree longitude as simulated by SD-WACCM-X. This is what a ground-based instrument over the tropics and at 0-degree longitude would observe. Figure 1A shows that for this sample case, temperature appears to be dominated by a 24-hour oscillation/ diurnal tide. On the other hand, figure 1B shows how a 12-hour oscillation/ semidiurnal tide could manifest alongside a diurnal tide. Between 90 km and 100 km, this zonal wind profile shows westerly winds over 4 am to 12 noon local-time and by easterly winds the rest of the day. If the diurnal tide dominated this region, periods of westerly winds and easterly winds should each last exactly 12 hours. Yet, here we see easterly winds dominating most of the day. This indicates that both diurnal and semidiurnal tides are strong. Figure 1C shows how an atmospheric parameter varies if the semidiurnal tide is most dominant. Between 80 km and 100 km, we can see southward winds occurring between midnight and 8 am local-time as well as between noon and 6 pm local-time. Northward winds occur over the other local times. While one can clearly determine the periodicities of the dominant tides from this perspective, one cannot determine the wavenumber of the tides.

Satellite-based observations can give you global coverage in a day but not full local-time coverage. One needs to utilize multiple months of data to attain full local-time coverage. Even then, one still must assume that tidal variabilities at daily timescales aren’t important. Currently,

only three-dimensional first-principles Physics-based models can give us both global coverage and full local-time coverage in a day. Until we develop the most ideal observational dataset, these models offer a satisfactory option to furthering our understanding of these tides.

2.1.2 Two-dimensional Least-squares Fit

To calculate the SW2 amplitudes and phases of a particular parameter, this work uses two dimensional least-squares fit. The fit uses basis functions of the following form (Wu et al, 1995):

$$X(\lambda, t) = \bar{X} + \sum_{n=1}^{3} \sum_{s=-4}^{4} \hat{X}_{n,s} \cos(n\Omega t - s\lambda - \hat{\psi}_{n,s}) + \sum_{s=1}^{4} \hat{X}_{s} \cos(s\lambda - \hat{\psi}_{s}) \quad (1)$$

Here, X is any atmospheric parameter. $\bar{X}$ is the daily-mean zonal-mean component of the parameter. The second summation term comprises of the migrating and non-migrating diurnal ($n = 1$), semidiurnal ($n = 2$) and terdiurnal ($n = 3$) tide components with wavenumbers (s) from -4 to 4. The third summation term comprises of the stationary planetary waves with wavenumbers from 1 to 4. $\hat{X}$ and $\hat{\psi}$ are the amplitudes and phases, respectively.

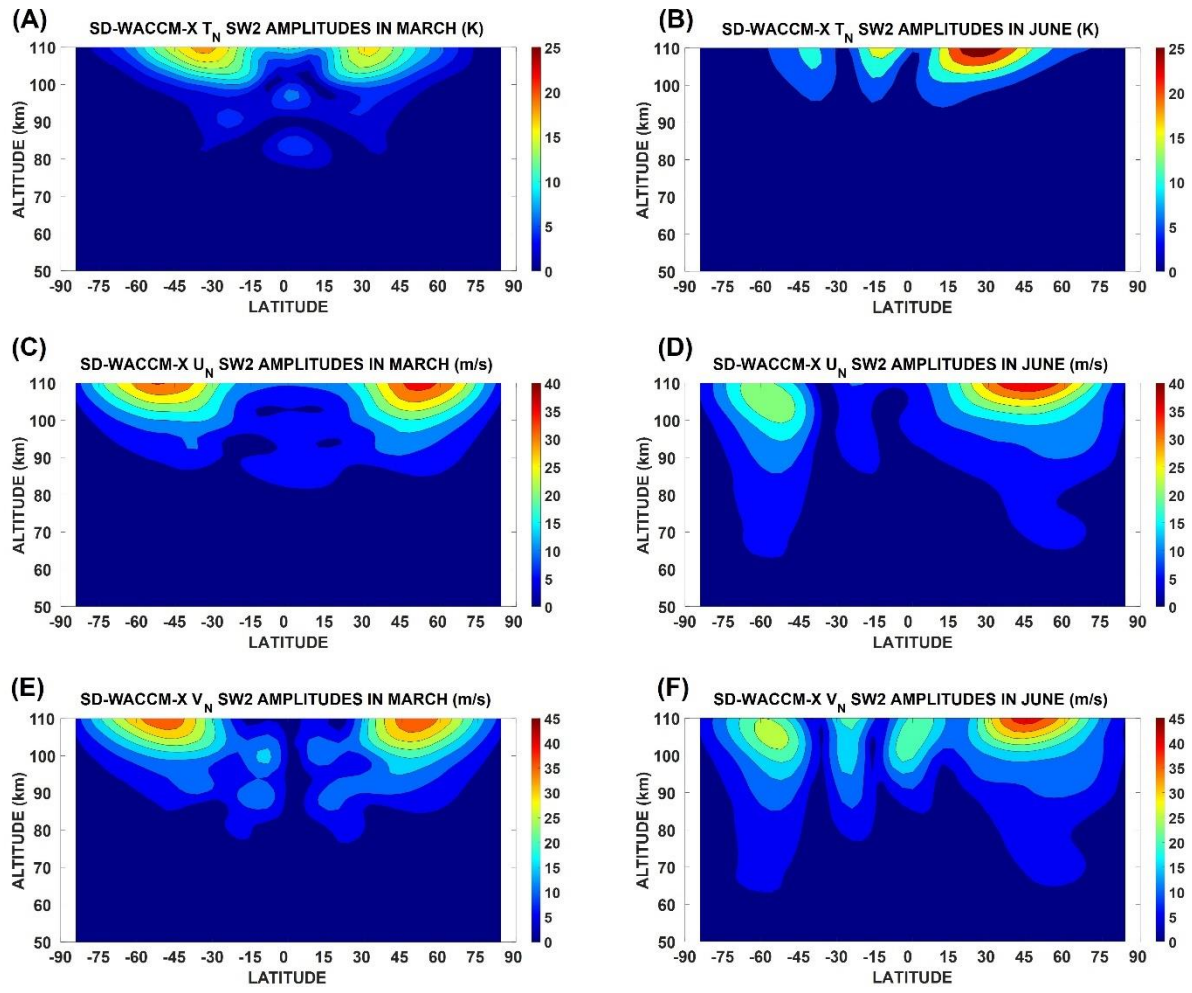

Figure 2: Migrating semidiurnal tide amplitudes of (A) temperature in March equinox, (B) temperature in June solstice, (C) zonal wind in March equinox, (D) zonal wind in June solstice, (E) meridional wind in March equinox and (F) meridional wind in June solstice.

Figure 2 shows sample calculations of SW2 amplitudes for temperature, zonal wind and meridional wind for both an equinox month and a solstice month in the mesosphere and lower thermosphere. Figure 2A shows the SW2 amplitudes for temperature in March equinox peaking above 100 km over the northern and southern mid-latitudes. Peak amplitudes reach around 20K. Figure 2B shows the SW2 amplitudes for temperature in June solstice peaking over the northern mid-latitudes with values reaching around 25K. Figure 2C shows the SW2 amplitudes for zonal

wind in March equinox peaking over the northern and southern high latitudes with values reaching around 35m/s. Figure 2D shows the SW2 amplitudes for zonal wind in June solstice peaking over the northern mid-latitudes with values reaching around 35m/s. Figure 2E shows the SW2 amplitudes for meridional wind in March equinox. It peaks over regions like where zonal-wind SW2 peaks in March equinox. Figure 2F shows the SW2 amplitudes for meridional wind in June solstice and it also peaks over regions like where zonal-wind SW2 peaks in June solstice. As mentioned above, previous studies have already extensively explored these regions of maximum amplitudes (Manson et al, 2002; Wu et al, 2011). This paper focuses on exploring the amplitudes over the low latitudes. Figure 2A shows a preview of this paper's focus. Figure 2A shows local maximum in temperature SW2 amplitudes over the low latitudes.

2.1.3 Hough Mode Reconstruction

To explain the seasonality of the SW2 components of tropical MLT temperature, zonal wind and meridional wind, we perform two model diagnostics. The first diagnostic is a Hough Mode reconstruction of these components. This involves reconstructing these SW2 components in terms of the 5 SW2 Hough modes shown in figure 3. Note that each dynamical parameter has its own set of Hough modes. Figure 3A shows the Hough modes for temperature. Figure 3B shows the Hough modes for zonal wind. Figure 3C shows the Hough modes for meridional wind. Classical linear tidal theory shows that a tide manifests as Hough modes. Hough modes are eigen-solutions to the linearized primitive equations in spherical coordinates assuming the background atmosphere is isothermal, and the zonal mean winds are zero. When tide-mean wind interactions are accounted for, linear tidal theory shows that the mode distortion can be reproduced by superimposing Hough modes according to the relative amplitudes demanded by orthogonal decomposition (Lindzen and Hong, 1974). Hence, this analysis determines if the

background atmosphere's distortion of these modes as they vertically propagate primarily drive the seasonality of the SW2 components of tropical MLT temperature, zonal wind and meridional wind.

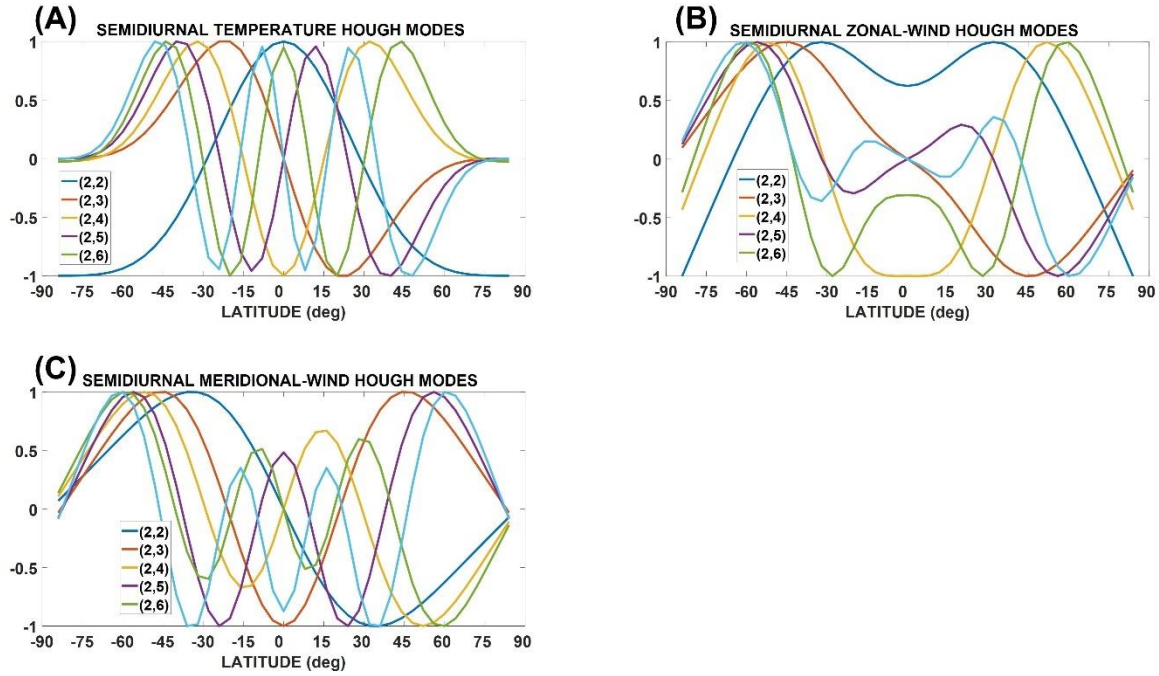

Figure 3: Semidiurnal temperature (A), zonal wind (B) and meridional wind (C) Hough modes. In these plots, the modes are normalized to have values solely between -1 and 1 but for the Hough mode reconstruction calculations, the modes are not normalized.

This process begins by decomposing the SW2 components of temperature, zonal wind and meridional wind into Hough modes. To present this process, we use the SW2 component of temperature as an example. We first take the latitude profile of tropical MLT region temperatures' SW2 amplitudes and phases $\bar{A}(\phi)$ and $\theta(\phi)$ at each altitude z, and construct a new latitude profile whose elements are a complex number $M(\phi) = Ai + B$ where $A = \bar{A}\cos(\frac{2\pi\theta}{12})$ and $B = \bar{A}\sin(\frac{2\pi\theta}{12})$. Then, we regress $M(\phi)$ with a Hough function indexed j. This

gives complex regression coefficients $\sigma_j(z)$ for each hough mode. This complex number is then used to calculate the amplitude and phase of each Hough mode component.

Also, we use these complex regression coefficients to construct a new latitude profile $M'(\phi)$ at each altitude z as $M'(\phi) = A'(\phi)i + B'(\phi) = \sum_{j=1}^{5} \sigma_j \Theta_j(\phi)$ where $\Theta(\phi)$ corresponds to a Hough function. This new latitude profile will have elements that are complex numbers. Finally, for each element in the profile, we take the complex number and calculate amplitudes and phases as $\bar{A}'(\phi) = \sqrt{A'^2(\phi) + B'^2(\phi)}$ and $\theta'(\phi) = \tan^{-1}\left[\frac{B\prime(\phi)}{A\prime(\phi)}\right]$. $\bar{A}'(\phi)$ and $\theta'(\phi)$ are the amplitudes and phases of the reconstructed SW2 component. The same process is applied to zonal wind and meridional wind's SW2 components.

2.1.4 Tendency Analysis of the Thermodynamic and Momentum Equation

The second diagnostic is a tendency analysis of the thermodynamic and momentum equations. The thermodynamic equation used in this tendency analysis is given by:

$$\frac{\partial T}{\partial t} = -\vec{V} \cdot \nabla T + \frac{\omega R T}{c_p P} + Q_{diab} \quad (2)$$

In this equation, T is temperature. t is time in seconds. ω is vertical velocity in Pa/s. P is atmospheric pressure in Pa. g is the acceleration due to gravity which is equal to 9.8 m/s^2. R is the gas constant for dry air which is equivalent to 287.058 J/kg/K. c_p is specific heat of dry air at constant pressure which is equivalent to 1005 J/kg/K. The left-hand-side of equation 2 is the time-derivative of temperature. The right-hand-side terms are the total advection term, adiabatic heating/cooling term and diabatic heating term. The diabatic heating term is the sum of chemical heating, Joule heating, long-wave heating, non-local thermodynamic equilibrium long-wave heating, short-wave heating, CO_2 near-IR heating, CO_2 IR cooling, NO IR cooling, extreme UV

heating, non-EUV photolysis heating and heating due to parameterized gravity waves. The goal of this tendency analysis is to determine what terms on the right-hand-side contributes the most to the SW2 amplitude of the time-derivative of temperature. This analysis begins by calculating all the terms in this equation and then calculating their SW2 amplitudes. The total advection term in this equation is calculated as:

$$F_{adv,T} = -V \cdot \nabla T = -\left(\frac{u}{a\cos\phi}\frac{\partial T}{\partial \lambda} + \frac{v}{a}\frac{\partial T}{\partial \phi} + w\frac{\partial T}{\partial z}\right) \quad (3)$$

In this equation, u is zonal wind, v is meridional wind and w is vertical wind all in m/s. ϕ is latitude. λ is longitude. z is log-pressure height. a is the Radius of Earth which is equal to 6.36×10^6 m. The terms in the right-hand-side are advection of temperature due to zonal-wind, meridional wind and vertical wind.

Advection is further split into linear and non-linear advection. To do this, we substitute $u = \bar{u} - u'$, $v = \bar{v} - v'$, $w = \bar{w} - w'$, $T = \bar{T} - T'$ into equation 3. Terms with overbars denote daily mean zonal-mean and primed terms are perturbations from the daily-mean zonal-mean. From the resulting equation, the linear advection term is this section of the equation:

$$F_{linAdv,T} = \frac{\bar{u}}{a\cos\theta}\frac{\partial T'}{\partial \lambda} + \frac{\bar{v}}{a}\frac{\partial T'}{\partial \theta} + \frac{v'}{a}\frac{\partial \bar{T}}{\partial \theta} + \bar{w}\frac{\partial T'}{\partial z} + w'\frac{\partial \bar{T}}{\partial z} \quad (4)$$

This equation shows that linear advection includes the advection of mean winds by temperature perturbations as well as the advection of temperature perturbations by the mean winds. Calculation of non-linear advection explicitly is difficult because it involves atmospheric wave decomposition. To determine the relative importance of non-linear advection, we opt to just compare the SW2 component of total advection and linear advection. Gu and Du (2018)

316 employed a similar analysis to determine the thermodynamic budget behind the migrating
317 diurnal tide.

318 The momentum equations used in this tendency analysis are given by:

319 $$\frac{\partial u}{\partial t} = fv - \frac{1}{\mathrm{a}\cos\lambda}\frac{\partial \Phi}{\partial \lambda} - \vec{V}\cdot\nabla \mathrm{u} + \frac{\mathrm{uv}}{\mathrm{a}}\tan\phi + F_{GW,x} \quad (5)$$

320 $$\frac{\partial v}{\partial t} = -fu - \frac{1}{a}\frac{\partial \Phi}{\partial \phi} - \vec{V}\cdot\nabla \mathrm{v} + \frac{\mathrm{u}^2}{\mathrm{a}}\tan\phi + F_{GW,y} \quad (6)$$

321 f is the Coriolis parameter. Φ is geopotential height. $F_{GW,x}$ and $F_{GW,y}$ are the gravity wave zonal
322 and meridional drag. Equation 5 is the momentum equation for zonal wind while equation 6 is
323 the momentum equation for meridional wind. For both cases, the terms on the right-hand-side are
324 the Coriolis force, pressure gradient force, advection, curvature and gravity wave drag. Like the
325 thermodynamic equation, our tendency analysis of the momentum equations determines what
326 terms on the right-hand-side contributes the most to the SW2 amplitude of the time-derivative of
327 zonal-wind and meridional wind. Thus, this will also involve calculating each term in this
328 equation and then calculating their SW2 amplitudes. The total advection terms are expressed as
329 follows:

330 $$F_{adv,x} = -V\cdot\nabla u = -\left(\frac{u}{\mathrm{a}\cos\phi}\frac{\partial u}{\partial \lambda} + \frac{v}{a}\frac{\partial u}{\partial \phi} + w\frac{\partial u}{\partial z}\right) \quad (7)$$

331 $$F_{adv,y} = -V\cdot\nabla v = -\left(\frac{u}{\mathrm{a}\cos\phi}\frac{\partial v}{\partial \lambda} + \frac{v}{a}\frac{\partial v}{\partial \phi} + w\frac{\partial v}{\partial z}\right) \quad (8)$$

332 The linear advection term is expressed as follows:

333 $$F_{linAdv,x} = -\vec{V}\cdot\nabla u = -\left(\frac{\bar{u}}{\mathrm{a}\cos\phi}\frac{\partial u'}{\partial \lambda} + \frac{\bar{v}}{a}\frac{\partial u'}{\partial \phi} + \frac{v'}{a}\frac{\partial \bar{u}}{\partial \phi} + \bar{w}\frac{\partial u'}{\partial z} + w'\frac{\partial \bar{u}}{\partial z}\right) \quad (9)$$

334 $$F_{linAdv,y} = -\vec{V}\cdot\nabla v = -\left(\frac{\bar{u}}{\mathrm{a}\cos\phi}\frac{\partial v'}{\partial \lambda} + \frac{\bar{v}}{a}\frac{\partial v'}{\partial \phi} + \frac{v'}{a}\frac{\partial \bar{v}}{\partial \phi} + \bar{w}\frac{\partial v'}{\partial z} + w'\frac{\partial \bar{v}}{\partial z}\right) \quad (10)$$

Like the tendency analysis with the thermodynamic equation, to determine the relative importance of non-linear advection in these horizontal winds, we opt to just compare the SW2 components of their total advection and linear advection terms. Lu et al (2012) employed a similar analysis to determine the momentum budget behind the migrating diurnal tide.

The results of these tendency analyses will complement the results of the Hough mode analysis. The argument that Hough modes can be used to mathematically express global tidal modes assumes that the tides in our atmosphere behave according to classical tidal theory. In classical tidal theory, it is assumed that temperature is only controlled by adiabatic heating/cooling while winds are only controlled by the Coriolis force and the pressure gradient force. Our Hough mode analysis only determines if the seasonality of tropical MLT temperature, zonal wind and meridional wind's SW2 components can be explained by classical tidal theory. Our tendency analysis will determine the specific classical or non-classical physical processes driving it.

2.2 Satellite Observations and Alias Test

2.2.1 Satellite Observations

For our alias test, this work utilizes the longitude and UT information of temperature observations from the Sounding of the Atmosphere using Broadband Emission Radiometry (SABER) instrument onboard the Thermosphere Ionosphere Mesosphere Energetics and Dynamics (TIMED) satellite as well as the Microwave Limb Sounder (MLS) onboard the NASA Aqua satellite. SABER has alternating latitudinal coverage of 82^{o}N – 53^{o}S and 53^{o}N – 82^{o}S that occurs due to the TIMED spacecraft yaw cycle every ~60 days (Russell et al, 1999). The mission has an orbital period of ~1.6 hours and a local time precession of 12 minutes per day. This orbit allows SABER to achieve full diurnal coverage after 60 days (Zhang et al, 2006). This work uses

SABER temperature longitude and UT information from profiles between day 60 and day 120 of year 2005. On the other hand, the Aura satellite is in a sun-synchronous orbit. The ascending nodes of the Aura orbit, when the spacecraft is moving toward the north, cross the equator at 1:45±15 PM (short-handed to 2PM hereafter) local time. Similarly, the descending nodes, when the spacecraft is moving toward the south, cross the equator at 1:45±15 AM (short-handed to 2AM hereafter) local time (https://aura.gsfc.nasa.gov/scinst.html). This orbit allows MLS to provide near-global maps of 2AM and 2PM temperature from the stratosphere to the upper mesosphere. This work utilizes the longitude and UT information of Aura MLS version 4.2x (V4.2x) temperature observations (https://mls.jpl.nasa.gov/data/v4-2_data_quality_document.pdf).

2.2.2 Alias Test

Following Wu et al (1995) and Forbes and Wu (2005), our alias test begins by synthesizing a test cosine signal using specified longitude and UT information. The signal is given by:

$$\mathrm{N}(\lambda, t) = \widehat{N}\cos(n\Omega t_{UT} - s\lambda) \quad (11)$$

Synthesizing this signal gives a set of profiles that are then subject to two-dimensional least-squares fit. However, instead of performing the fit across a spectrum of waves simultaneously, the fit is performed across a spectrum of waves individually.

3. Results and Discussion

3.1 Seasonal Climatology of SD-WACCM-X temperature, zonal wind and meridional wind's SW2 Component

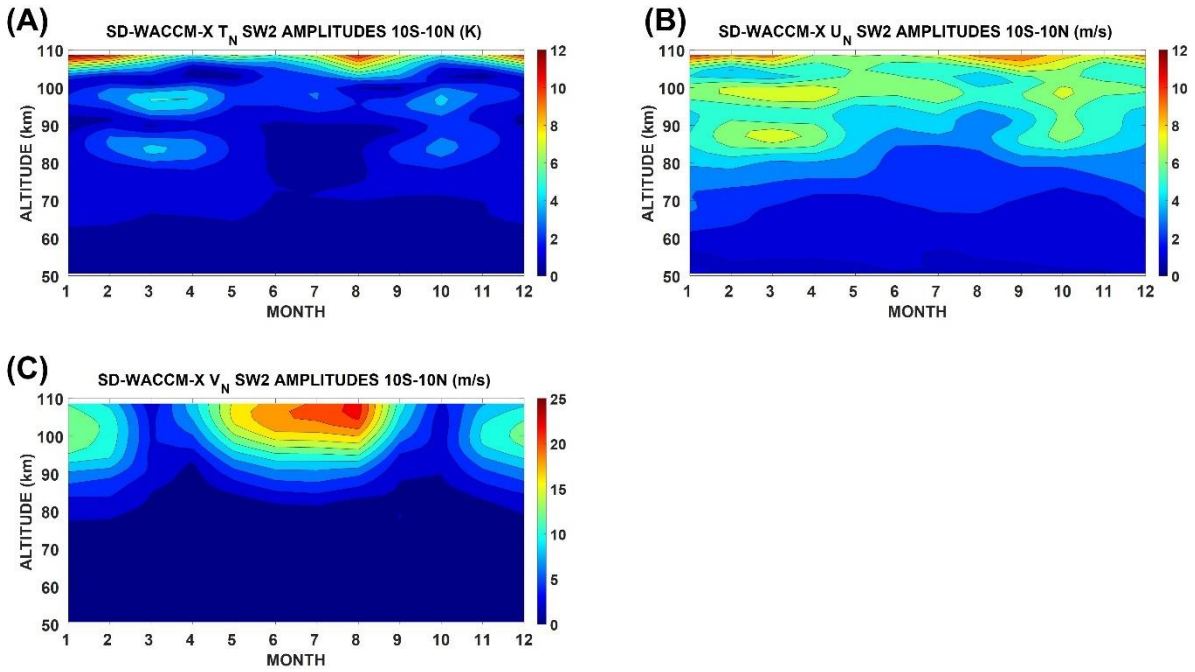

Figure 4: Seasonality of the migrating semidiurnal tide components of tropical upper mesosphere and lower thermosphere temperature (top row), zonal wind (middle row) and meridional wind (bottom row). The amplitudes are on the left column and the phases are on the right column. They are all functions of altitude and month. Units are specified on the plots.

To calculate the seasonal climatology of tropical UMLT temperature, zonal wind and meridional wind's SW2 component, we first averaged SD-WACCM-X simulated temperature, zonal wind and meridional wind between latitudes 10S and 10N. Then, from these, we calculate their SW2 amplitudes and phases using 2D least-squares fit. Figure 4 shows the seasonal climatology of the SW2 component of temperature, zonal wind and meridional wind averaged between latitudes 10S and 10N. Figures 4A and 4B show that the seasonality of tropical UMLT temperature and zonal-wind's SW2 amplitudes both exhibit a seasonality characterized by the appearance of two local amplitude peaks between 75 km and 105 km during equinox seasons. In March equinox, temperature's (zonal wind's) SW2 amplitudes first show a local peak of around 5

K (7 m/s) at ~87 km, then another local peak of around 7 K (7 m/s) at ~97 km before reaching its highest amplitudes with values greater than 12 K (12 m/s) above 105 km. The peaks around ~97 km extends into July but with a weaker value. The amplitudes in October are lower than the March equinox amplitudes by around 1 to 2K (1 to 2 m/s). On the other hand, figure 4C shows that the meridional wind's SW2 amplitude solely peak during solstice seasons with largest amplitudes of around 20 m/s at ~105 km in August.

As mentioned earlier, numerous studies using ground-based instruments have observed the presence of at least one peak in the amplitudes of the 12-hour oscillation component of zonal and meridional winds in this same region before the amplitude reaches its largest values above 105 km (Reddi and Ramkumar, 1997; Vincent et al, 1998; Manson et al, 1999; Deepa et al, 2006). Du et al (2007) confirmed using CMAM simulations that the SW2 component does contribute to these 12-hour oscillations. However, nobody has presented observations that temperature's SW2 component also has the same features. Our work here indicates that temperature's SW2 component may also have such features.

Past studies have shown that these features can only be reproduced by three-dimensional models (Du et al, 2007; Ravis et al, 2013). Tidal models cannot reproduce this. Hence, it is argued that classical linear tidal theory isn't enough to fully explain the presence of one or two local amplitude peaks in the SW2 component of tropical UMLT zonal wind and meridional wind. However, no work has tried to determine the mechanisms behind these peaks. Although the features aren't the same as those seen in the 12-hour components of horizontal winds, these results still indicate that SD-WACCM-X can be used to understand the mechanisms behind these peaks. Hence, for the remainder of this paper, we focus on explaining these local amplitude

peaks. We first explain the double amplitude peak in March equinox. Then, we explain the single peak in June solstice.

3.2 March equinox double peak

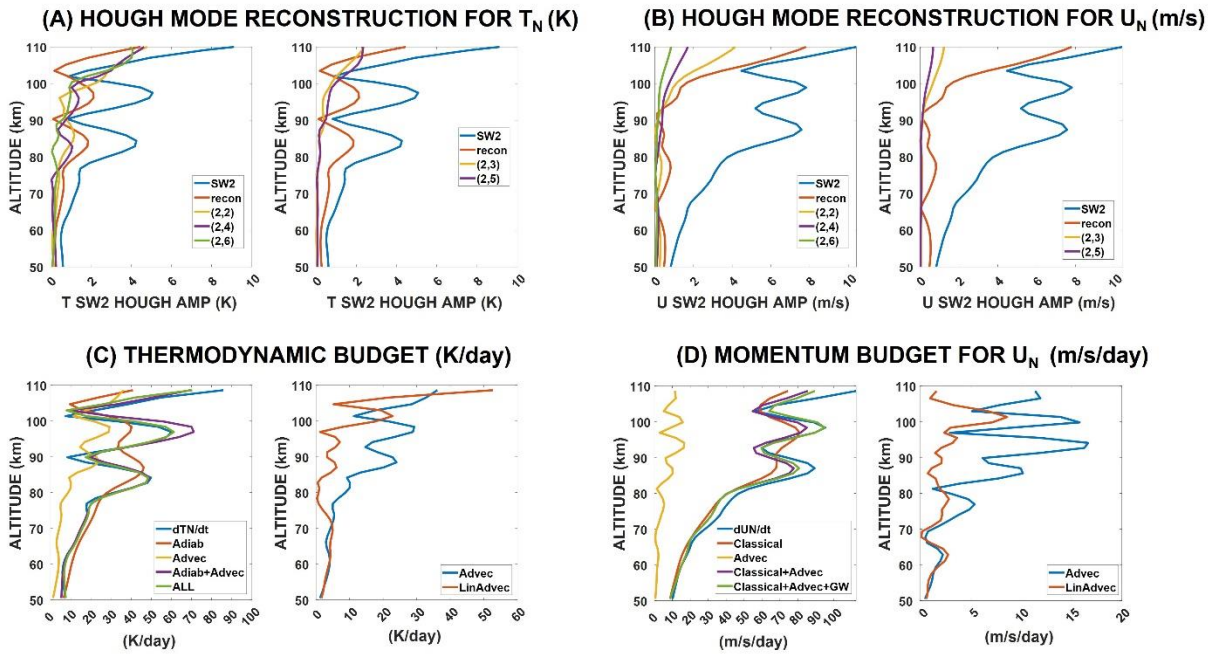

Figure 5: Hough mode reconstruction as well as Hough mode component amplitudes for the migrating semidiurnal tide in tropical UMLT temperature (A) and in tropical UMLT zonal wind during March equinox (B). Migrating semidiurnal tide amplitudes of the individual terms in the thermodynamic equation (C) and zonal momentum equation (D) over the tropical UMLT region during March equinox. See text for more details. Units are specified on the plots.

Figure 5 shows the results of our Hough mode reconstruction and tendency analysis to explain the March equinox double peaks in SD-WACCM-X temperature and zonal-wind SW2 amplitudes. We only show the analysis for these two variables because this double peak structure is only present in them. We first present the results of our Hough mode reconstruction. Figure 5A

shows two subplots. The subplot on the left shows the vertical profile of the amplitude of tropical UMLT temperature's SW2 component in March equinox, the amplitudes of the symmetric SW2 Hough modes and the amplitude of temperature SW2 reconstructed from all Hough modes (hereafter referred to as reconstructed temperature SW2). The subplot on the right shows the vertical profile of the amplitude of tropical UMLT temperature's SW2 component in March equinox, the amplitudes of the asymmetric SW2 Hough modes and the amplitude of the reconstructed temperature SW2. Figure 5A shows that the reconstructed temperature SW2's profile also shows a double peak structure, but the amplitudes are around half of the actual double peak structure. Of all the modes, only the (2,4) mode shows a double peak structure found at the altitudes of the double peak structure in tropical UMLT temperature SW2. The (2,2) mode shows a single local peak at around 85 km. The (2,2) and (2,4) mode have the largest amplitudes of all the modes with the (2,2) mode showing comparable amplitudes to the (2,4) mode between 85 km and 90 km. These indicate that for the reconstructed temperature SW2, the (2,4) mode is primarily behind the local peak at around 95 km while both (2,2) and (2,4) mode are primarily behind the local peak at around 85 km. However, since the reconstructed profile's amplitudes are only half of the actual profile's amplitudes, these results indicate that these Hough modes cannot fully explain this double peak structure in tropical UMLT temperature's SW2 amplitude during March equinox.

Figure 5B shows the same as figure 5A but for the zonal wind. Figure 5B clearly shows that the reconstruction doesn't reproduce any hint of the double peak structure. Thus, figure 5A and 5B clearly show that mode distortion or mode coupling cannot fully explain these local amplitude peak structures. These results indicate that this double-peak structure during March equinox in the SW2 component of tropical temperature and zonal-wind is not primarily due to

452 the distortion of SW2 modes by the background atmosphere. This implies that wave-mean flow
453 interaction is not a primary driver of these peaks.

454 Now we show the results of our tendency analysis with the thermodynamic equation.
455 Figure 5C shows two subplots. The subplot on the left shows the SW2 amplitude of $\frac{dT_n}{dt}$, the SW2
456 amplitude of the adiabatic term, the total advection term, the adiabatic term plus the total
457 advection term and the SW2 amplitude of the sum of all the terms in the thermodynamic
458 equation except $\frac{dT_n}{dt}$. The subplot on the right shows the SW2 amplitudes of temperature total
459 advection and temperature linear advection. This figure shows that the sum of all terms in the
460 thermodynamic equation can satisfactorily reproduce $\frac{dT_n}{dt}$. Looking at the adiabatic terms, we find
461 that the sum of the adiabatic heating due to vertical motion and total advection can reproduce the
462 double-peak structure although the higher peak has a slightly larger amplitude. However, if you
463 look at each term individually, the adiabatic term has a higher amplitude than the total advection
464 term. The adiabatic term shows two peaks, but the features are significantly different from the
465 peaks of $\frac{dT_n}{dt}$. This indicates that the double peak structure in SW2 temperature requires, at the
466 very least, the sum of both the adiabatic term and total advection term. For the peak at 95 km, it
467 is further shown that diabatic heating terms allow it to match best with the $\frac{dT_n}{dt}$ peak. Figure 5C
468 also shows the contribution of linear advection on the total advection. Linear advection cannot
469 fully explain the total advection. Non-linear advection is important.

470 Finally, we show the results of our tendency analysis with the zonal wind momentum
471 equation. Figure 5D also shows two subplots like figure 5C. The subplot on the left shows the
472 SW2 amplitude of tropical UMLT $\frac{dU_n}{dt}$, the classical terms (sum of Coriolis force and pressure

gradient term), the total advection term, the classical term plus total advection term and the SW2 amplitudes of the sum of the classical term, total advection term and gravity wave drag. The subplot on the right shows the SW2 amplitudes of zonal wind total advection and zonal wind linear advection. This figure shows that the sum of all terms in the zonal wind momentum equation can satisfactorily reproduce $\frac{dU_n}{dt}$. Breaking down the terms, this figure shows that the classical terms have the largest contributions, but the features don't satisfactorily match with $\frac{dU_n}{dt}$. This means the winds simply due to the pressure gradient and the Coriolis force won't immediately drive the double-peak structure in zonal wind. The amplitude of total advection is almost an order of magnitude lower than the classical terms. However, this figure shows that you still need advection to at least reproduce a double-peak structure that is close to the double-peak structure of $\frac{dU_n}{dt}$. It is also shown that linear advection cannot fully reproduce the total advection term implying that non-linear advection is important. Adding the gravity waves cause the peak at around 95 km to match perfectly with the peak of $\frac{dU_n}{dt}$ while it also improves the peak at around 90 km.

For both the double peak structure in temperature SW2 and zonal wind SW2, our results indicate the importance of non-linear advection. Non-linear advection involves wave-wave interaction. For the double peak structure in zonal wind SW2, apart from wave-wave interaction, our results also indicate the importance of gravity wave drag. The Hough mode reconstruction earlier suggested that wave-mean flow interaction isn't a primary driver. Our tendency analysis adds that in-situ forcing due to wave-wave interaction and even gravity waves may be important.

3.3 June solstice single peak

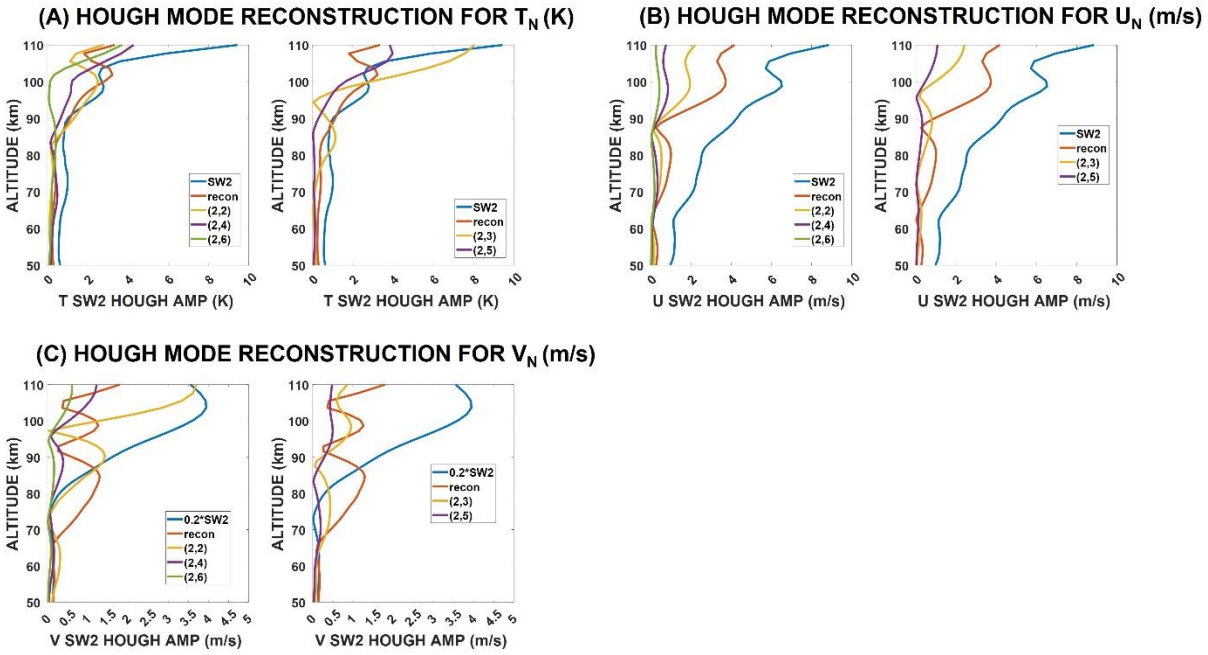

494

495 *Figure 6: Hough mode reconstruction as well as Hough mode component amplitudes for the*
496 *migrating semidiurnal tide in tropical UMLT temperature (A), in tropical UMLT zonal wind (B)*
497 *and in tropical UMLT meridional wind (C) during June solstice. See text for more details. Units*
498 *are specified on the plots.*

499 Figure 6A shows the same as figure 5A but for June solstice. Figure 6A shows that the
500 reconstructed temperature SW2's profile reproduces a peak but at a different altitude. The peak
501 in tropical UMLT temperature SW2's amplitude is located between 95 km and 100 km while the
502 peak in the reconstructed temperature SW2's profile is located between 100 km and 105 km. Of
503 all the modes, the (2,2) and (2,3) mode have the largest amplitudes between 95 km and 105 km.
504 These results indicate that these Hough modes cannot fully explain this single peak structure in
505 tropical UMLT temperature's SW2 amplitude during June solstice.

506 Figure 6B shows the same as figure 5B but for June solstice. Figure 6B shows that the
507 reconstructed zonal wind SW2's profile only partially reproduces the peak in zonal wind SW2's

amplitude. The reconstructed amplitudes are just lower by 2 m/s. Of all the modes, the (2,2) Hough mode has the largest amplitude followed by the (2,4) Hough mode. These results also indicate that these Hough modes cannot fully explain this single peak structure in tropical UMLT zonal wind's SW2 amplitude during June solstice.

Figure 6C shows the same as figure 6B but for meridional wind. Note that the SW2 amplitude of meridional wind is reduced by a factor of 0.2 because the region of peak amplitude above 90 km is 5 times larger than the Hough mode amplitudes. Figure 6C shows that the reconstructed meridional wind SW2's profile cannot reproduce the peak in meridional wind SW2's amplitude. Figures 6A, 6B and 6C clearly indicate that this single peak structure during June solstice in the SW2 component of tropical temperature, zonal-wind and meridional wind is not primarily due to the distortion of SW2 modes by the background atmosphere. This implies that wave-mean flow interaction is not a primary driver of these peaks. This is the same as the double peak structure in March equinox temperature SW2 and zonal wind SW2.

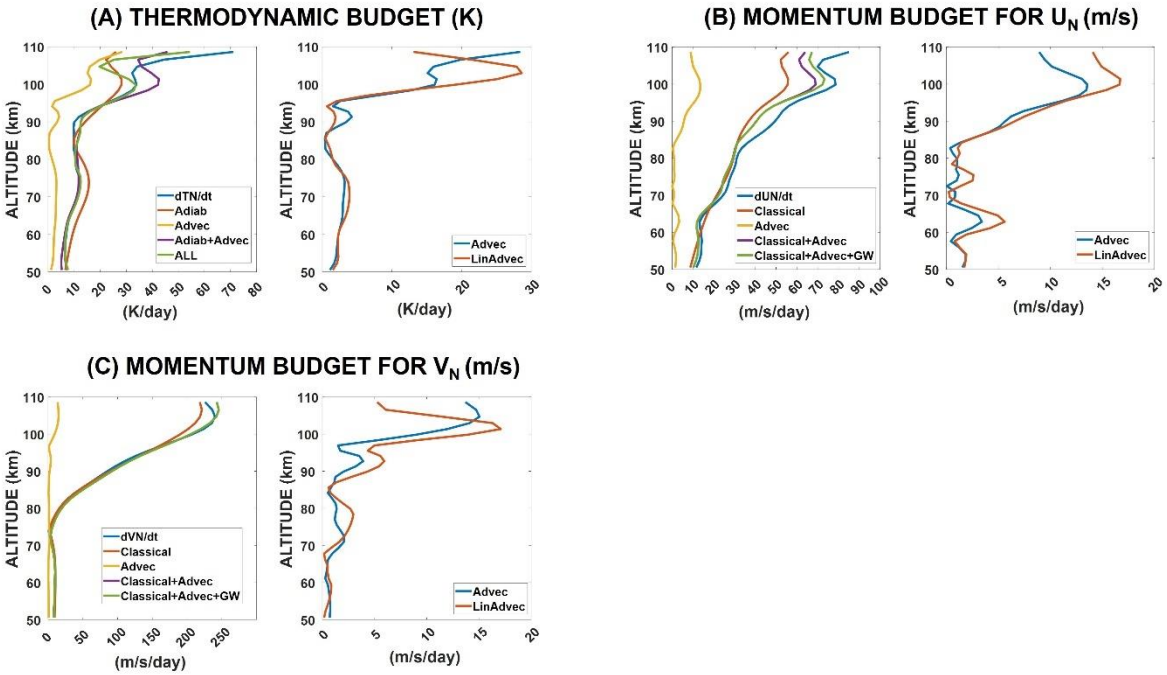

522

523 *Figure 7: Migrating semidiurnal tide amplitudes of the individual terms in the thermodynamic*
524 *equation (A), zonal momentum equation (B) and meridional momentum equation (C) over the*
525 *tropical UMLT region during June solstice. See text for more details. Units are specified on the*
526 *plots.*

527 Now we show the results of our tendency analysis with the thermodynamic equation.
528 Figure 7A shows the same as figure 5C but for June solstice. This figure shows that unlike the
529 double peak structure in March equinox temperature SW2, the single peak structure in June
530 solstice temperature SW2 requires all the terms in the thermodynamic equation to satisfactorily
531 reproduce $\frac{dT_n}{dt}$. The sum of the adiabatic term and total advection term can produce the local peak
532 at around 100 km, but the amplitude is larger than the correct amplitude by around 10 K/day.
533 The diabatic term is needed to significantly reduce this difference. Figure 7A also shows the
534 contribution of linear advection on the total advection. Linear advection alone can capture a

local-peak above 95 km, but it peaks at around 105 km. Also, the amplitude is higher by 10 K/day. This indicates that non-linear advection is important.

We next show the results of our tendency analysis with the zonal wind momentum equation. Figure 7B shows the same as figure 5D but for June solstice. This figure shows that the sum of all terms in the zonal wind momentum equation can satisfactorily reproduce $\frac{dU_n}{dt}$. Breaking down the terms, this figure shows that the classical terms have the largest contributions, and it does capture the peak at around 100 km although the amplitude is only half the correct amplitude. The amplitude of total advection is almost an order of magnitude lower than the classical terms but combining it with the adiabatic term significantly increases the amplitudes. Figure 7B also shows that linear advection can only partially capture the general structure of the total advection especially the peak at around 100 km. The amplitude of the linear advection term is larger than the total advection term by around 5 m/s/day. Thus, non-linear advection is also important. When the classical terms and advection are combined, the profile improves with the amplitude only 15 m/s/day lower than the correct amplitude. When gravity waves are added, the difference is further reduced to 10 m/s/day.

Finally, we show the results of our tendency analysis with the meridional wind momentum equation. Figure 7C shows the same as figure 7B but for meridional wind. This figure shows that the sum of all terms in the meridional wind momentum equation can satisfactorily reproduce $\frac{dV_n}{dt}$. Breaking down the terms, figure 7C shows that the classical terms have the largest contributions, and it does capture the peak at around 100 km with the amplitude already around 85% of the correct amplitude. The amplitude of total advection is two orders of magnitude lower than the classical terms but when it is added to the classical terms, the

amplitude matches the amplitude of $\frac{dV_n}{dt}$. Linear advection can capture the general structure of the total advection especially the peak at around 100 km, but the amplitude is larger. Thus, non-linear advection is also important. When gravity waves are added, the difference is negligible. This indicates the gravity wave drag on the meridional direction isn't important.

Like the double peak structure in March equinox, our results indicate that non-linear advection and therefore wave-wave interaction is also very important in driving the single peak structure in temperature SW2, zonal wind SW2 and meridional wind SW2 during June solstice. For the single peak structure in temperature SW2 during June solstice, apart from wave-wave interaction, our results also indicate the importance of diabatic heating terms. For the single peak structure in zonal wind SW2 during June solstice, apart from wave-wave interaction, our results also indicate the importance of gravity wave drag. The Hough mode reconstruction earlier suggested that wave-mean flow interaction also isn't a primary driver for these single peak structures. Our tendency analysis adds that in-situ forcing due to wave-wave interaction, gravity waves and diabatic heating may be important.

3.4 Alias Test

The previous sections have shown that wave-wave interaction, gravity waves and diabatic heating are likely significant contributors to SW2's seasonal variability in the tropical UMLT. Wave-wave interaction and gravity waves are difficult to observe and predict. Since our results suggest that these variabilities may be tied to the presence of SW2 in the tropical UMLT region, we need to be very careful in making assumptions on the presence of SW2 in the tropical UMLT region. Here, we quantify how carelessly ignoring SW2 can affect the calculation of daily-mean zonal-mean as well as tides in the tropical UMLT region. This is done through an alias analysis.

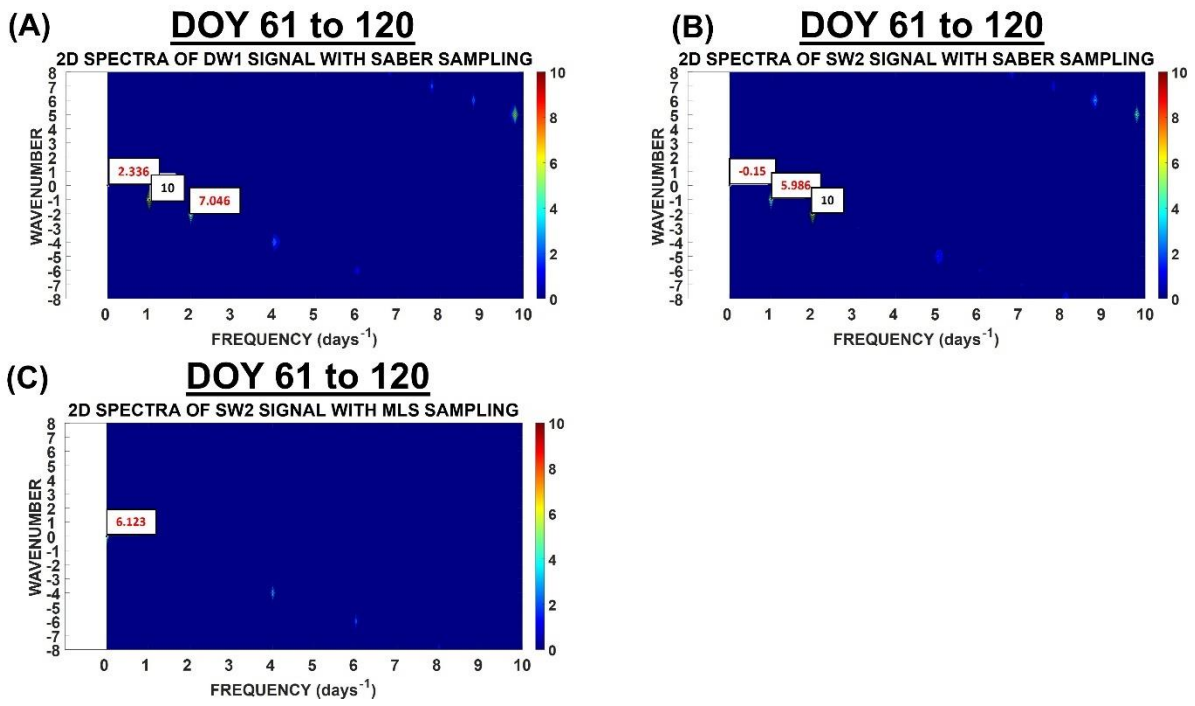

Figure 8: Alias spectra for a DW1 signal (A) and an SW2 signal (B) with amplitude 0 and uses SABER longitude-UT sampling. Alias spectra for an SW2 signal (C) with amplitude 0 and uses MLS longitude-UT sampling.

Our alias analysis involves synthesizing a signal using the longitude and UT sampling of a particular observational platform. Here, we use SABER and MLS' longitude and UT sampling. In figure 8A, we synthesized a DW1 signal with 0 daily mean zonal-mean but an amplitude of 10 of arbitrary units using SABER's longitude and UT sampling over the tropics and over 60 days centered on March equinox. From this sampling, we then use 2D least-squares fit to scan across all these planetary-scale waves and tides to get their amplitudes. The spectrum is given in this figure 8A. Here we can see that for wavenumber -1 and frequency 1 per day which corresponds to DW1, we get the expected amplitude of 10. At the same time, we find that even if the signal contained no daily-mean zonal-mean, there is a daily-mean zonal-mean of ~2. There is also an SW2 signal of ~7. These indicate that with SABER's sampling, DW1 can induce a ~20% error in

daily-mean zonal-mean values and ~70% error in SW2 amplitudes. In figure 8B, we synthesized an SW2 signal with 0 daily mean zonal-mean but an amplitude of 10 using SABER's sampling. Figure 8B reveals that this sampling generates a fake DW1 signal with an amplitude of ~6 which corresponds to a ~60% error. In figure 8C, we synthesize the same SW2 signal but using MLS' sampling. Figure 8C reveals that this sampling generates a fake daily-mean zonal-mean of around 6 which corresponds to a ~60% error.

Most studies that have estimated tides using 2D least-squares fit always perform the fit across a spectrum, so these errors are mitigated. But we do have a wide range of other methods now that don't employ 2D least-squares fit because their target is the short-term variability of these waves. Our analysis here suggests that over the tropics, these methods must be careful to account for the presence of SW2.

4. Discussions

This work shows that the SD-WACCM-X simulated seasonality of the SW2 components of tropical UMLT temperature, zonal wind and meridional wind are characterized by the presence of local peaks in their amplitudes. During equinox seasons, the SW2 component of tropical UMLT temperature and zonal wind have a double-peak structure. During June solstice, the SW2 component of UMLT temperature, zonal wind and meridional wind have a single peak structure. Similar features were found in ground-based observations of the 12-hour component of zonal and meridional wind (Reddi and Ramkumar, 1997; Vincent et al, 1998; Manson et al, 1999; Deepa et al, 2006). These were also reproduced by other three-dimensional models (Du et al, 2007; Ravis et al, 2013). Thus, this work took advantage of SD-WACCM-X's ability to reproduce this to give explanations to the presence of these peaks.

For both the double peak structure and single peak structure in tropical UMLT temperature SW2 and zonal wind SW2, our Hough mode reconstruction suggests that these cannot simply be driven by the background atmosphere's distortion of SW2 Hough modes. Our tendency analysis suggests that in-situ generation by wave-wave interaction and gravity waves may be playing major roles. For the single peak structure in the SW2 component of tropical UMLT temperature, zonal wind and meridional wind during June solstice, our Hough mode reconstruction also suggests that this cannot simply be driven by the background atmosphere's distortion of SW2 Hough modes. These suggested mechanisms for the seasonality of SW2 in the tropics is very different from the suggested mechanisms for the seasonality of SW2 in the middle to high latitudes. Pedatella et al (2020) and van Caspel et al (2021) found that the seasonality of SW2 in the middle to high latitudes can be explained by the background atmosphere's distortion of SW2 modes originating from the stratosphere. However, these do not mean that our results contradict with their results. Tidal variability due to wave-mean flow interaction and due to wave-wave interaction can both occur simultaneously in global-scales.

The lower boundary of the Thermosphere Ionosphere Electrodynamics General Circulation model is set at around 97 km and the conditions either come from the Global Scale Wave Model or the CTMT model (Roble et al, 1988; Richmond et al, 1992; Qian et al, 2014; Jones Jr, et al, 2014). The GSWM model does account for gravity wave effects in the form of eddy diffusion, but it does not account for wave-wave interaction nor gravity wave drag (Hagan and Forbes, 2002; 2003). CTMT assumes all tidal variability can be expressed as Hough mode extensions (Oberheide et al, 2011). Thus, CTMT assumes SW2 comes from the lower atmosphere and its variability at ~97 km is primarily driven by wave-mean flow interaction. Our results suggest that these lower boundary conditions are still valid if one is only interested in

SW2 variability due to wave-mean flow interaction as well as global-scale phenomena. However, they may not be enough if one would like to also account for SW2 variability due to in-situ forcing particularly from wave-wave interaction as well as phenomena solely over the tropics.

Our alias analysis indicates that the zonal-mean component over the tropics as estimated from MLS' sampling may contain alias from SW2 if SW2 has significant amplitude in the region. Taken together with our results showing that SW2 is closely tied with short-term variability phenomena like wave-wave interaction and gravity waves, our work indicates that one needs to be very careful when calculating the zonal-mean component over the tropics from sun-synchronous satellite observations. One cannot simply assume that SW2's amplitudes are negligible.

5. Summary and Conclusions

This modeling study uses the SD-WACCM-X model to determine and explain the seasonality of SW2 in tropical UMLT temperature, zonal-wind and meridional-wind. This work also quantifies how much SW2 affects tidal decomposition using satellite observations. SD-WACCM-X outputs from 2001 to 2019 are used and from these outputs, this work constructs a seasonal climatology of the monthly-mean of all parameters (e.g., temperature, winds, etc). Then, these parameters are used to determine and explain the seasonal climatology of tropical UMLT temperature, zonal wind and meridional wind's SW2 component.

This work does two model diagnostics. The first diagnostic is a Hough mode reconstruction of SW2 amplitudes in the tropical E-region. This determines if the seasonality of SW2 in the tropical E-region can be explained by the background atmosphere distortion of SW2

660 modes coming from the lower atmosphere. The second diagnostic is a tendency analysis of the
661 thermodynamic and momentum equations. With the thermodynamic equation, this tendency
662 analysis determines the contributions of linear advection, non-linear advection, adiabatic
663 heating/cooling and diabatic heating terms. With the zonal wind and meridional wind momentum
664 equations, this tendency analysis determines the contributions of classical terms which include
665 Coriolis force and pressure gradient term as well as the non-classical terms which include linear
666 advection, non-linear advection and gravity wave drag.

667 Results show that the seasonal climatology of tropical UMLT temperature, zonal wind
668 and meridional wind's SW2 component are marked by two features in their amplitudes. One is a
669 double peak structure in SW2 temperature and zonal-wind amplitude during equinox seasons.
670 The other is a single peak structure in SW2 temperature, SW2 zonal-wind and SW2 meridional
671 wind in June solstice.

672 Hough mode reconstruction reveals that for the double-peak structure in March equinox
673 temperature and zonal wind, it cannot be fully reproduced by a linear combination of 5 SW2
674 Hough modes. Tendency analysis for the March equinox temperature double peak structure
675 reveals that it requires, at minimum, both the adiabatic heating/cooling term and the advection
676 term combined. It is further revealed that linear advection alone cannot reproduce the total
677 advection indicating that non-linear advection is important. Tendency analysis for the March
678 equinox zonal wind double peak structure reveals that, at minimum, it requires the classical
679 terms and the advection terms. And, like temperature, linear advection alone cannot reproduce
680 the total advection. If you include gravity wave drag, the fit is even more improved. Similar
681 mechanisms were found for the June solstice single peak. From these model diagnostics, this
682 work concludes that Hough functions aren't a good representation of the seasonality of tropical

683 UMLT SD-WACCM-X temperature SW2, zonal wind SW2 and meridional wind SW2 because
684 in-situ generation by wave-wave interaction and/or by gravity waves play a significant role.
685 Their seasonality isn't primarily driven by the background atmosphere's distortion of its vertical
686 propagation. Since these mechanisms are related to short-term variability, this work further
687 suggests that SW2's presence in the tropical UMLT is difficult to observe and predict.

688 Results of our alias analysis indicates that the DW1 component estimated using SABER's
689 sampling in the tropics may have an alias equal to ~60% of SW2's amplitudes. It also indicates
690 that the daily-mean zonal-mean component estimated using MLS' sampling in the tropics may
691 have an alias also equal to ~60% of SW2's amplitudes. From this alias analysis, this work
692 concludes that satellite observations with SABER and MLS' sampling is prone to SW2-related
693 aliasing. Our diagnostics suggest that SW2's presence in the tropical UMLT is difficult to
694 observe and predict, the alias analysis further suggests that one cannot simply assume SW2 in the
695 tropical UMLT is negligible. Future work will determine what specific atmospheric waves could
696 be involved in the wave-wave interactions driving these seasonal features.

697 **Acknowledgements**

698 CCJHS and LCC acknowledge Taiwan National Science and Technology Council (NSTC)
699 grants 111-2636-M-008-004, 107-2923-M-008-001-MY3, and 110-2923-M-008-005-MY3, as
700 well as the Higher Education SPROUT grant to the Center for Astronautical Physics and
701 Engineering from the Taiwan Ministry of Education. The work of DLW and JNL was supported
702 by NASA's TSIS Project and Sun-Climate research. LQ acknowledges support from the
703 following NASA grants: 80NSSC19K0278, 80NSSC20K0189, NNH19ZDA001N-HGIO and
704 NNH19ZDA001N-HSR. HL acknowledges support from NASA grant 80NSSC20K1323.
705 National Center for Atmospheric Research is a major facility sponsored by the National Science

706 Foundation under Cooperative Agreement No. 1852977. CCJHS is supported by the Taiwan
707 NSTC grants and acknowledges high-performance computing support from Cheyenne
708 (doi:10.5065/D6RX99HX) provided by NCAR's Computational and Information Systems
709 Laboratory, sponsored by the National Science Foundation. As a component of the Community
710 Earth System Model, WACCM-X source code are publicly available at
711 http://www.cesm.ucar.edu. The SABER dataset presented in this paper are accessible from the
712 SABER website: http://saber.gats-inc.com/data.php. The MLS dataset presented in this paper are
713 accessible from the MLS website: https://aura.gsfc.nasa.gov/mls.html.

714 **References**

715 Angelats i Coll, M. and J. M. Forbes, Nonlinear interactions in the upper atmosphere: The s = 1
716 and s = 3 nonmigrating semidiurnal tides, J. Geophys. Res., 107, 1157,
717 doi:10.1029/2001JA900179, 2002.

718 Burrage, M. D., Hagan, M. E., Skinner, W. R., Wu, D. L., & Hays, P. B. (1995a). Long-term
719 variability in the solar diurnal tide observed by HRDI and simulated by the GSWM. *Geophysical*
720 *Research Letters*, *22*(19), 2641-2644.

721 Burrage, M. D., Wu, D. L., Skinner, W. R., Ortland, D. A., & Hays, P. B. (1995b). Latitude and
722 seasonal dependence of the semidiurnal tide observed by the high-resolution Doppler
723 imager. *Journal of Geophysical Research: Atmospheres*, *100*(D6), 11313-11321.

724 Chang, L. C., Palo, S. E., & Liu, H. L. (2011). Short-term variability in the migrating diurnal tide
725 caused by interactions with the quasi 2 day wave. *Journal of Geophysical Research:*
726 *Atmospheres*, *116*(D12).

727 Davis, R. N., Du, J., Smith, A. K., Ward, W. E., & Mitchell, N. J. (2013). The diurnal and
728 semidiurnal tides over Ascension Island (° S, 14° W) and their interaction with the stratospheric
729 quasi-biennial oscillation: studies with meteor radar, eCMAM and WACCM. *Atmospheric*
730 *Chemistry and Physics*, *13*(18), 9543-9564.

731 Deepa, V., Ramkumar, G., Antonita, M., Kumar, K. K., & Sasi, M. N. (2006, November).
732 Vertical propagation characteristics and seasonal variability of tidal wind oscillations in the MLT
733 region over Trivandrum (8.5 N, 77 E): First results from SKiYMET meteor radar. In *Annales*
734 *Geophysicae* (Vol. 24, No. 11, pp. 2877-2889). Copernicus GmbH.

735 Du, J., Ward, W. E., Oberheide, J., Nakamura, T., & Tsuda, T. (2007). Semidiurnal tides from
736 the extended Canadian Middle Atmosphere Model (CMAM) and comparisons with TIMED
737 Doppler interferometer (TIDI) and meteor radar observations. *Journal of atmospheric and solar-*
738 *terrestrial physics*, *69*(17-18), 2159-2202.

739 Forbes, J. M. and D. Wu, Solar tides as revealed by measurements of mesosphere temperature by
740 the MLS experiment on UARS, J. Atmos. Sci., 63, 1776–1797, 2006.

741 Forbes, J. M., & Vial, F. (1989). Monthly simulations of the solar semidiurnal tide in the
742 mesosphere and lower thermosphere. *Journal of atmospheric and terrestrial Physics*, *51*(7-8),
743 649-661.

744 Forbes, J. M., & Zhang, X. (2017). The quasi-6 day wave and its interactions with solar
745 tides. *Journal of Geophysical Research: Space Physics*, *122*(4), 4764-4776.

746 Forbes, J. M., Atmospheric tides 2. The solar and lunar semidiurnal components, J. Geophys.
747 Res., 87, 5241–5252, 1982.

748 Forbes, J. M., N. A. Makarov, and Yu. I. Portnyagin, First results from the meteor radar at South
749 Pole: A large 12-hour oscillation with zonal wavenumber one, Geophys. Res. Lett., 22, 3247–
750 3250, 1995.

751 Forbes, J. M., X. Zhang, S. Palo, J. Russell, C. J. Mertens, and M. Mlynczak, Tidal variability in
752 the ionospheric dynamo region, J. Geophys. Res., 113, A02310, doi:10.1029/2007JA012737,
753 2008.

754 Gu, H., & Du, J. (2018). On the roles of advection and solar heating in seasonal variation of the
755 migrating diurnal tide in the stratosphere, mesosphere, and lower
756 thermosphere. *Atmosphere*, *9*(11), 440.

757 Limpasuvan, V., Orsolini, Y. J., Chandran, A., Garcia, R. R., & Smith, A. K. (2016). On the
758 composite response of the MLT to major sudden stratospheric warming events with elevated
759 stratopause. *Journal of Geophysical Research: Atmospheres*, **121**, 4518–
760 4537. https://doi.org/10.1002/2015JD024401

761 Lindzen, R. S. and S.-S. Hong, Effects of mean winds and meridional temperature gradients on
762 solar and lunar semidiurnal tides in the atmosphere, J. Atmos. Sci., 31, 1421–1466, 1974.

763 Liu, H. L., Bardeen, C. G., Foster, B. T., Lauritzen, P., Liu, J., Lu, G., ... & Qian, L. (2018a).
764 Development and Validation of the Whole Atmosphere Community Climate Model With
765 Thermosphere and Ionosphere Extension (WACCM-X 2.0). *Journal of Advances in Modeling*
766 *Earth Systems*, *10*(2), 381-402.

767 Liu, J., H.-L. Liu, W. Wang, A. G. Burns, Q. Wu, Q. Gan, S. C. Solomon, D. R. Marsh, L. Qian,
768 G. Lu, N. M. Pedatella, J. M. McInerney, J. M. Russell III, and W. S. Schreiner (2018b), First

769 results from the ionospheric extension of WACCM-X during the deep solar minimum year of
770 2008, *J. Geophys. Res.*, 123, doi:10.1002/2017JA025010.

771 Lu, X., Liu, H. L., Liu, A. Z., Yue, J., McInerney, J. M., & Li, Z. (2012). Momentum budget of
772 the migrating diurnal tide in the Whole Atmosphere Community Climate Model at vernal
773 equinox. *Journal of Geophysical Research: Atmospheres*, *117*(D7).

774 Manson, A., Meek, C., Hagan, M., Hall, C., Hocking, W., MacDougall, J., ... & Burrage, M.
775 (1999). Seasonal variations of the semi-diurnal and diurnal tides in the MLT: Multi-year MF
776 radar observations from 2 to 70 N, and the GSWM tidal model. *Journal of Atmospheric and*
777 *Solar-Terrestrial Physics*, *61*(11), 809-828.

778 Marsh, D. R., Mills, M. J., Kinnison, D. E., Lamarque, J. F., Calvo, N., & Polvani, L. M. (2013).
779 Climate change from 1850 to 2005 simulated in CESM1 (WACCM). *Journal of climate*, *26*(19),
780 7372-7391.

781 Oberheide, J., Hagan, M. E., & Roble, R. G. (2003). Tidal signatures and aliasing in temperature
782 data from slowly precessing satellites. *Journal of Geophysical Research: Space*
783 *Physics*, *108*(A2).

784 Oberheide, J., Wu, Q., Killeen, T. L., Hagan, M. E., & Roble, R. G. (2007). A climatology of
785 nonmigrating semidiurnal tides from TIMED Doppler Interferometer (TIDI) wind data. *Journal*
786 *of atmospheric and solar-terrestrial physics*, *69*(17-18), 2203-2218.

787 Palo, S. E., R. G. Roble, and M. E. Hagan, Middle atmosphere effects of the quasi two-day wave
788 determined from a General Circulation Model, Earth Planets Space, 51, 629–647, 1999.

Pancheva, D., Mukhtarov, P., & Andonov, B. (2009, February). Global structure, seasonal and interannual variability of the migrating semidiurnal tide seen in the SABER/TIMED temperatures (2002–2007). In *Annales Geophysicae* (Vol. 27, No. 2, pp. 687-703). Copernicus GmbH.

Pedatella, N. M., & Forbes, J. M. (2010). Evidence for stratosphere sudden warming-ionosphere coupling due to vertically propagating tides. Geophysical Research Letters, 37(11). https://doi.org/10.1029/2010GL043560

Reddi, C. R., & Ramkumar, G. (1997). Climatologies of tidal winds in the radio-meteor region over Trivandrum (8 N). *Journal of Atmospheric and Solar-Terrestrial Physics*, *59*(14), 1757-1777.

Rienecker, M. M., Suarez, M. J., Gelaro, R., Todling, R., Bacmeister, J., Liu, E., ... & Woollen, J. (2011). MERRA: NASA's modern-era retrospective analysis for research and applications. *Journal of climate*, *24*(14), 3624-3648.

Russell, J. M., III, M. G. Mlynczak, L. L. Gordley, J. J. Tansock Jr., and R. W. Esplin (1999), Overview of the SABER experiment and preliminary calibration results, SPIE Proc., 3756, 277–288, doi:10.1117/12.366382.

Teitelbaum, H. and F. Vial, On tidal variability induced by nonlinear interaction with planetary waves, J. Geophys. Res., 96, 14,169–14,178, 1991.

Teitelbaum, H., F. Vial, A. H. Manson, R. Giraldez, and M. Massbeuf, Non-linear interaction between the diurnal and semidiurnal tides: terdiurnal and diurnal secondary waves, J. Atmos. Terr. Phys., 51, 627–634, 1989.

van Caspel, W. E., Espy, P. J., Ortland, D. A., & Hibbins, R. E. (2022). The Mid-to High-Latitude Migrating Semidiurnal Tide: Results From a Mechanistic Tide Model and SuperDARN Observations. *Journal of Geophysical Research: Atmospheres*, *127*(1), e2021JD036007.

Vincent, R. A., Kovalam, S., Fritts, D. C., & Isler, J. R. (1998). Long-term MF radar observations of solar tides in the low-latitude mesosphere: Interannual variability and comparisons with the GSWM. *Journal of Geophysical Research: Atmospheres*, *103*(D8), 8667-8683.

Walterscheid, R. L. and S. V. Venkateswaran, Influence of mean zonal motion and meridional termperature gradients on the solar semidiurnal atmospheric tide: A spectral study, Part 1, Theory, J. Atmos. Sci., 36, 1623–1635, 1979a.

Walterscheid, R. L. and S. V. Venkateswaran, Influence of mean zonal motion and meridional termperature gradients on the solar semidiurnal atmospheric tide: A spectral study, Part 2, Numerical results, J. Atmos. Sci., 36, 1636–1662, 1979b.

Wu, D. L., Hays, P. B., & Skinner, W. R. (1995). A least squares method for spectral analysis of space-time series. *Journal of Atmospheric Sciences*, *52*(20), 3501-3511.

Wu, Q., Killeen, T. L., Nozawa, S., McEwen, D., Guo, W., & Solomon, S. C. (2003). Observations of mesospheric neutral wind 12-hour wave in the Northern Polar Cap. *Journal of atmospheric and solar-terrestrial physics*, *65*(8), 971-978.

Wu, Q., Ortland, D., Solomon, S., Skinner, W., & Niciejewski, R. (2011). Global distribution, seasonal, and inter-annual variations of mesospheric semidiurnal tide observed by TIMED TIDI. Journal of Atmospheric and Solar-Terrestrial Physics, 73(17), 2482–2502. https://doi.org/10.1016/j.jastp.2011.08.007

832 Yamashita, K., S. Miyahara, Y. Miyoshi, K. Kawano, and J. Ninomiya, Seasonal variation of
833 non-migrating semidiurnal tide in the polar MLT region in a general circulation model, J. Atmos.
834 Sol.-Terr. Phys., 64, 1083–1094, 2002.

835 Yuan, T., Schmidt, H., She, C. Y., Krueger, D. A., & Reising, S. (2008). Seasonal variations of
836 semidiurnal tidal perturbations in mesopause region temperature and zonal and meridional winds
837 above Fort Collins, Colorado (40.6 N, 105.1 W). *Journal of Geophysical Research:*
838 *Atmospheres*, *113*(D20).

839 Zhang, X., Forbes, J. M., Hagan, M. E., Russell III, J. M., Palo, S. E., Mertens, C. J., &
840 Mlynczak, M. G. (2006). Monthly tidal temperatures 20–120 km from TIMED/SABER. *Journal*
841 *of Geophysical Research: Space Physics*, *111*(A10).

842 Zhang, J., Limpasuvan, V., Orsolini, Y. J., Espy, P. J., & Hibbins, R. E. (2021). Climatological
843 Westward-Propagating Semidiurnal Tides and Their Composite Response to Sudden
844 Stratospheric Warmings in SuperDARN and SD-WACCM-X. *Journal of Geophysical Research:*
845 *Atmospheres*, *126*(3), e2020JD032895.

846